Direct Instantaneous Force Control With Improved Efficiency for Four-Quadrant Operation of Linear Switched Reluctance Actuator in Active Suspension System

Zhu Zhang, *Student Member, IEEE*, N. C. Cheung, *Senior Member, IEEE*, K. W. E. Cheng, *Senior Member, IEEE*, Xiangdang Xue, *Member, IEEE*, and Jiongkang Lin

***Abstract*—A direct instantaneous force control with improved efficiency for the linear switched reluctance actuator (LSRA) is proposed in this paper. Four-quadrant operation is investigated for application in the active suspension system. Force ripple minimization is considered as the primary objective due to the direct impact on passenger ride comfort. An adaptive force distribution function based on the instantaneous force feedback is proposed to achieve a ripple-free system. The choice of switching parameters for improved operation efficiency is examined. The optimal switching positions are online adjusted with respect to the force demand. Simulation and experimental results are presented to verify the effectiveness of the proposed control strategy.**

***Index Terms*—Active suspension system, direct instantaneous force control (DIFC), force distribution function (FDF), linear switched reluctance actuator (LSRA).**

I. Introduction

ELECTROMAGNETIC active suspension systems have been introduced in vehicle applications over the past decade and have become a more competitive candidate than their hydraulic counterparts. To date, various electromagnetic actuators have been proposed by researchers and companies [1]–[4], and the permanent magnetic actuator was extensively investigated for its high force density. The structure of the electromagnetic active suspension system from Bose Corporation is shown in Fig. 1. However, the permanent magnet is quite expensive and tends to lose magnetization as the temperature rises.

A linear switched reluctance actuator (LSRA)-based electromagnetic active suspension system has the advantages of robust structure, low cost, high reliability, and fast dynamic response [5]. Moreover, LSRA can be operated in regenerating mode as well. The kinetic energy, which is dissipated to heat in passive suspensions, can be recovered back to the power source or provided to other instruments under certain circumstance [6], [7]. The regenerative power can compensate for the energy consumption and improve the overall efficiency of the active suspension system.

Fig. 1. Electromagnetic active suspension system.

However, the inherent force ripple of LSRA will degrade the performance of active suspensions, particularly the passenger ride comfort. Therefore, a high-performance control technique for force ripple minimization is critical for the active suspension system. The energy consumption is another important issue for the potential application of active suspensions in electric vehicle, which has a direct impact on the travel range. The problem can be improved by reducing the copper loss during operation.

LSRA has been studied in many applications, such as automation machine [8] and elevator [9]. Most applications are concerned about position control [10], [11], whereas the control objective in the active suspension system is to track the force demand generated from the suspension controller. There are primarily two types of techniques for force control. One is regarded as indirect method that the required force is converted to equivalent current demand and controlled by regulating the excitation current [12], [13]. The other way is direct instantaneous force control (DIFC), which considers the instantaneous force as a control variable and directly counteracts the force error [14]. Hence, fast dynamic response and good capability to eliminate the force ripple can be obtained.

This paper presents an improved DIFC that incorporates force distribution function (FDF), instantaneous force estimation, and online determination of switching positions. FDF is

Manuscript received October 25, 2011; revised January 9, 2012; accepted January 25, 2012. Date of publication February 23, 2012; date of current version May 9, 2012. This work was supported by the Innovation and Technology Fund of Hong Kong SAR under Project ITP/025/09AP. The review of this paper was coordinated by Prof. A. Khaligh.

The authors are with the Electrical Engineering Department, The Hong Kong Polytechnic University, Kowloon, Hong Kong (e-mail: ee.zz@connect.polyu.hk; norbert.cheung@polyu.edu.hk; eeecheng@polyu.edu.hk).

Color versions of one or more of the figures in this paper are available online at http://ieeexplore.ieee.org.

Digital Object Identifier 10.1109/TVT.2012.2188822

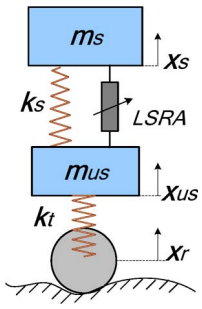

Fig. 2. Quarter-car model of electromagnetic suspension system.

considered to be an effective way to alleviate the problem of force ripple when there is an overlap of effective force region between adjacent phases. The estimated forces are not only feedbacked for hysteresis force control but also provided to improve the FDF. Since the primary goal of LSRA control is precise traction of force demand and force ripple minimization, the operation efficiency is subjected to the force dynamics. In the premise of ensuring acceptable force ripple, the energy efficiency of both motoring and regenerating mode is optimized by online adjusting the turn-ON and turn-OFF positions as the variation of force demand.

II. Four-Quadrant Operation of Linear Switched Reluctance Actuator

A. System Description

To simplify the analysis of electromagnetic suspension system and determine the operation mode for LSRA, a quarter car model is used, as shown in Fig. 2. Although the roll and pitch behaviors are eliminated, the fundamental performance of the suspension system can be evaluated. The quarter-car model of the electromagnetic suspension system consists of a linear spring and an LSRA supporting the sprung mass together. The tire is modeled as a spring of high stiffness acting on both unsprung and sprung masses.

The dynamic motion can be represented by the following equations:

$$m_s\ddot{x}_s + k_s(x_s - x_{us}) = u \tag{1}$$

$$m_{us}\ddot{x}_{us} - k_s(x_s - x_{us}) + k_t(x_{us} - x_r) = -u \tag{2}$$

where m_s and m_{us} are the sprung and unsprung masses, x_s and x_{us} are the displacements of the respective masses, k_s and k_t are the spring stiffness, u is the active force, and x_r represents the road disturbance.

B. Configuration of LSRA

For potential application in commercial vehicles, the volume of the LSRA should be compact enough to install in the limited space, without major modification to the vehicle structure. Double-sided LSRA has the advantage of higher force density than single-sided structure [5], and four double-sided LSRA modules can be arranged in a more compact configuration because the lateral forces by both sides of the stator are eliminated. Moreover, the elimination is helpful to reduce the acoustic noise during the operation [15].

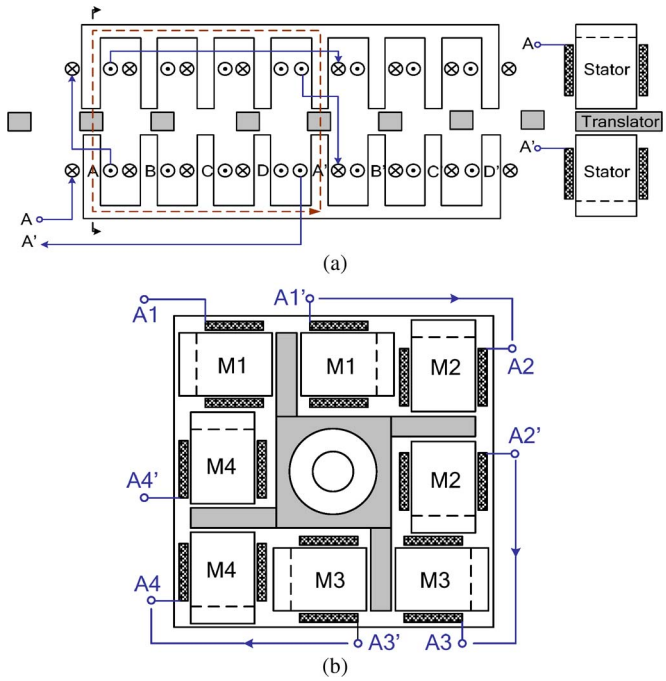

Fig. 3. Topology of proposed LSRA. (a) Double-sided LSRA module. (b) Cross-section of proposed LSRA.

Fig. 3(a) shows the configuration of the double-sided module, which is made of four phases with eight pairs of stator poles and eight translator poles. Four coils per phase are connected in series. The translator weight is considerably reduced due to the absence of excitation windings and back iron. The cross-section of the proposed LSRA is demonstrated in Fig. 3(b). It is composed of four identical double-sided LSRA modules. The translators per module are connected together by a hollow shaft, where the spring can be placed. The coils of the same phase from four modules are connected in series, whereas the magnetic circuit of each module is independent.

C. Operation Principle

The equivalent circuit is always used to analyze the dynamic performance of the LSRA and helpful for understanding the operation. Neglecting the mutual inductance between phases, the corresponding voltage equation is then given by

$$V = Ri + \frac{d\lambda(i,x)}{dt} = Ri + L\frac{di}{dt} + i\frac{dL}{dx}\frac{dx}{dt} \tag{3}$$

$$e = \frac{dx}{dt}\cdot i\frac{dL}{dx} = vi\frac{dL}{dx} \tag{4}$$

where V is the applied voltage, i is the phase current, R is the phase resistance, L is the phase inductance, λ is the flux linkage per phase, e is the back emf, v is the movement speed, and x is the translator position. It can be observed that the sign of e is determined by dL/dx. If phase winding is excited after the unaligned position, where the variation of phase inductance is positive, $dL/dx > 0$, the LSRA operates in motoring mode. If the phase winding is excited after the aligned position, where the variation of phase inductance is negative, $dL/dx < 0$, the LSRA operates in regenerating mode. The variation of

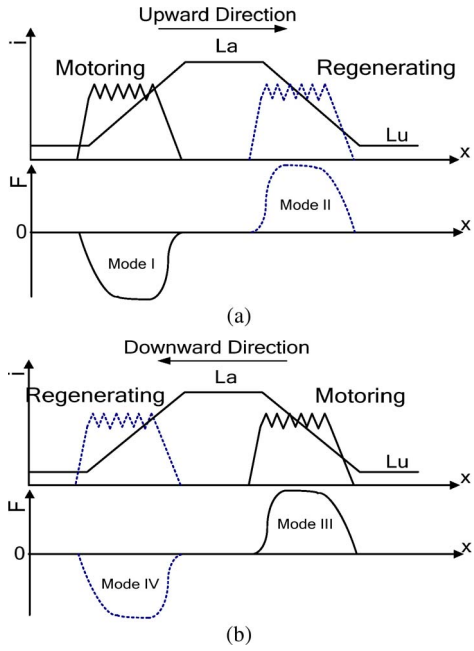

Fig. 4. Four-quadrant operation.

TABLE I
SWITCHING CONDITIONS OF OPERATION MODE

Suspension Deflection	Relative Velocity	Active Force	Operation Mode
$x_s - x_{us} > 0$	$\dot{x}_s - \dot{x}_{us} \geq 0$	Stretch	Motoring
	$\dot{x}_s - \dot{x}_{us} < 0$		Regenerating
$x_s - x_{us} < 0$	$\dot{x}_s - \dot{x}_{us} \geq 0$	Contraction	Regenerating
	$\dot{x}_s - \dot{x}_{us} < 0$		Motoring
$x_s - x_{us} = 0$	$\dot{x}_s - \dot{x}_{us} = 0$	Null	Standby

inductance and force with translator position is illustrated in Fig. 4. Considering the motion direction, four-quadrant operation is achieved by regulating the excitation sequence and switching position of each phase.

The switching condition of four operation modes depends on the suspension deflection and relative velocity of the sprung and unsprung masses, as shown in Table I. For example, the suspension deflection and the relative velocity become positive as the wheel falling into a sunken obstacle. To reduce the downward acceleration of sprung mass, an active stretching force is needed to support the sprung mass and prevent it from falling. The actuator operates at motoring mode during this stage. After the wheel reaches the bottom and moves upward, the relative velocity turns negative. A damping force is generated by the actuator, and the mechanical energy can be recovered by operating in regenerating mode. A similar situation with negative suspension deflection goes for the raised obstacle.

The stator and translator of LSRA are connected to the unsprung and sprung masses, respectively. Hence, the regenerative energy is captured when there is relative movement between the sprung and unsprung masses due to the road irregularities. The experimental setup of the quarter-car model with the proposed LSRA is demonstrated in Fig. 5.

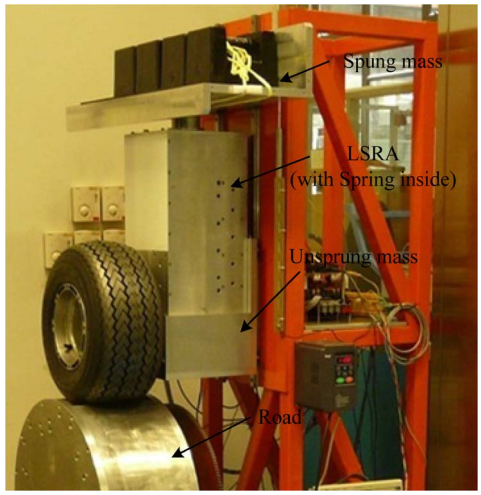

Fig. 5. Experimental setup of quarter-vehicle model.

D. Optimization Criteria

Although the force ripple is the dominant criterion of LSRA control for suspension application, other operation criteria, for example, the efficiency, are also critical for system performance. The efficiency has a direct impact on the energy consumption of vehicles, particularly for the electric vehicles. Therefore, to obtain a high-performance active suspension system, the force ripple and operation efficiency are selected as the optimization criteria in this paper.

For the simplicity of calculation, the force ripple in this paper is defined as the ratio of the difference between the maximum and minimum forces to the maximum force, which can be written as

$$F_R = \frac{F_{\max} - F_{\min}}{F_{\max}} \times 100\%. \tag{5}$$

Copper loss is the energy dissipated by the resistance of phase winding and contributes to a large decrease of the actuator efficiency. It increases as the square of the Root Mean Square (RMS) phase current $I_{\rm rms}$ and is given by

$$Pcu = mI_{\rm rms}^2 R \tag{6}$$

where m is the number of phase, and R is the resistance of the phase winding. Therefore, it is justified to examine the efficiency by the value of RMS phase current.

III. DIRECT INSTANTANEOUS FORCE CONTROL

The proposed DIFC scheme for LSRA is composed of the FDF, the force estimation unit, the hysteresis force controller, and the online determination unit of the switching position. The structure of this scheme is demonstrated in Fig. 6. The FDF is implemented to distribute the total force demand among four phases. The force reference per phase is varied with the translator position, but the sum of four individual values is equivalent to the total force demand at any position. Before the incoming phase is energized, the actuator force is contributed by the outgoing phase with the reference of the total force demand. The force references of the remaining three phases are

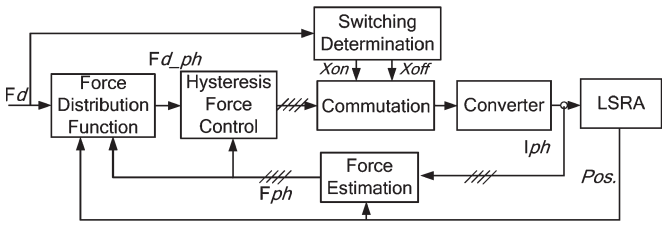

Fig. 6. Structure of DIFC.

determined as zero. When entering the effective force region of the incoming phase, the force demand of the outgoing phase is slowly reduced following the given function, and that of the incoming phase is increased accordingly. The total force demand is distributed between these two adjacent phases until the outgoing phase is turned OFF. The rest of the two phases are turned OFF during this stage. By this means, four individual phase demands are generated and then compared with the estimated force of the corresponding phase, respectively. The switching signals are generated by the hysteresis controller in accordance to the force errors and driving sequence. Although the acceptable force ripple can be achieved within a wide range of switching positions, the efficiency can be improved by optimizing the turn-ON and turn-OFF positions. Moreover, the optimal switching positions are varied with the force demand. The selection of the optimal value can be realized by the online determination scheme.

A. Force Estimation

The accuracy of force estimation directly decides the performance of the DIFC. However, the nonlinearity and discontinuous mode of operation make the relationship between the force and excitation current too complex to express in an analytical equation. The force depends not only on the excitation current but also on the translator position as well. Therefore, the look-up table and neural network are the most practical ways to online estimate the instantaneous force, and the look-up table is more favorable in real-time application due to the lower computation time [14], [16]–[18].

In this paper, the measured force characteristics as a function of excitation current and translator position are used to develop the look-up table, as presented in Fig. 7. By ignoring the mutual coupling effects and minor error between phases induced from manufacturing, the characteristic of the single phase is used to decrease the size of the look-up table [5], [19]–[21]. Furthermore, the negative force value can be omitted from the table and predicted from the symmetrical positive force. The interpolation algorithm is used to estimate the rest values among the measured points stored in the look-up table.

B. FDF

The effective force regions of neighboring phases are overlapped to ensure the two-phase excitation simultaneously during the phase commutation. It makes the FDF an effective way to reduce the force ripple. By distributing the force demand between two neighboring phases, the phase force is individually regulated and varied smoothly with the translator position.

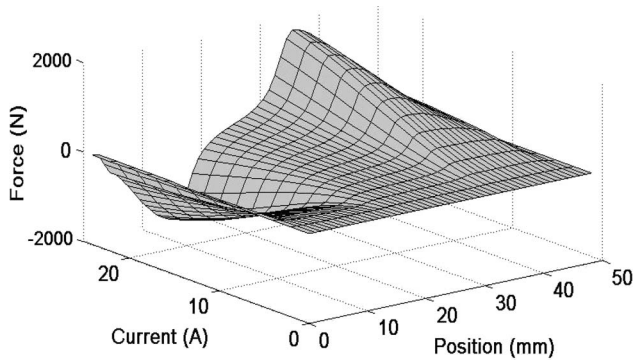

Fig. 7. Force characteristics.

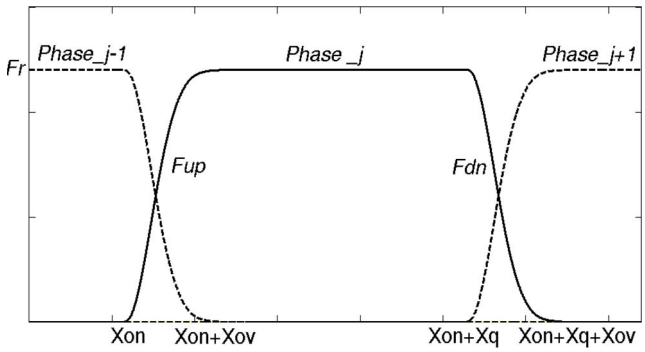

Fig. 8. Typical profile of exponential FDF.

Since there is no unique option for distribution function, a great many FDFs, such as linear, cubic, sinusoidal, and exponential function, have been proposed and studied by previous researchers [22]–[25]. Among these four FDFs, the exponential FDF is considered to be a better choice for improving both the efficiency and the speed range [26]. The typical profile of exponential FDF is shown in Fig. 8 and can be expressed by

$$\mathrm{FDF}_j(x) = \begin{cases} 0, & 0 \le x \le x_{\mathrm{on}} \\ F_{\mathrm{up\_}j}(x), & x_{\mathrm{on}} \le x \le x_{\mathrm{on}} + x_{\mathrm{ov}} \\ F_r, & x_{\mathrm{on}} + x_{\mathrm{ov}} \le x \le x_{\mathrm{on}} + x_q \\ F_{\mathrm{dn\_}j}(x), & x_{\mathrm{on}} + x_q \le x \le x_{\mathrm{on}} + x_q + x_{\mathrm{ov}} \\ 0, & x_{\mathrm{on}} + x_q + x_{\mathrm{ov}} \le x \le x_p \end{cases} \tag{7}$$

where x_{on} denotes the turn-ON position, x_{ov} is the overlap region, x_q and x_p are the stroke and translator pole pitch, F_r is the total force demand, and $F_{\mathrm{up\_}j(x)}$ and $F_{\mathrm{dn\_}j(x)}$ represent the function of the rising and declining portions, which can be written as

$$F_{\mathrm{up\_}j}(x) = F_r \left[1 - \exp\left(\frac{-(x - x_{\mathrm{on}})^2}{x_{\mathrm{ov}}}\right)\right] \tag{8}$$

$$F_{\mathrm{dn\_}j}(x) = F_r \left[\exp\left(\frac{-(x - x_{\mathrm{on}} - x_q)^2}{x_{\mathrm{ov}}}\right)\right]. \tag{9}$$

However, force ripple minimization cannot be achieved by exponential FDF over a wide range of switching positions. It can be observed from Fig. 9 that significant force ripple is generated during commutation with exponential FDF. To obtain a high-performance force control, an adaptive exponential FDF based on the force estimator is proposed in this paper.

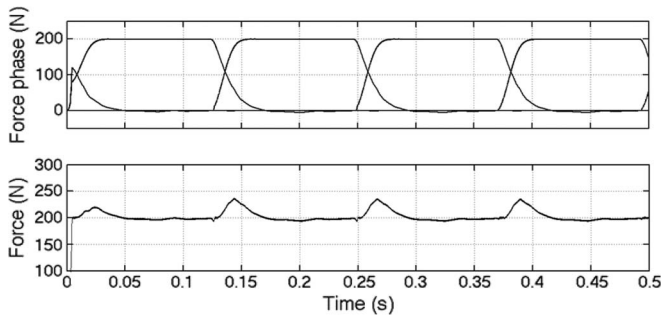

Fig. 9. Force profile with exponential FDF.

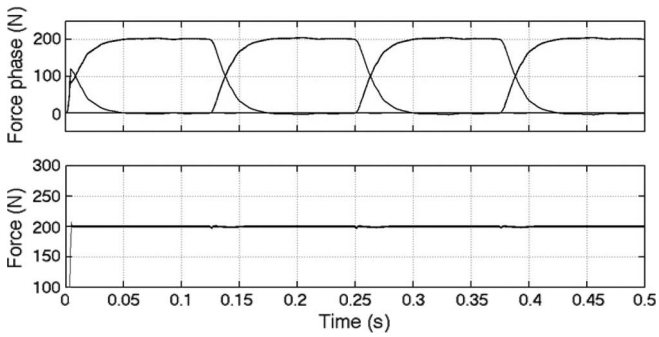

Fig. 10. Force profile with proposed adaptive FDF.

Compared with the conventional exponential FDF, the proposed FDF can distribute the total force adaptively between two adjacent phases in real time. The discrepancy between the total force demand and the output force can be minimized, and hence, the force ripple can be reduced.

During the overlap region, the force demand of the outgoing phase changes with the translator position in the form of the exponential function, which is the same as the conventional exponential FDF. However, the force demand of the incoming phase is adaptively varied with the difference between the total force demand and the estimated force of the outgoing phase. By this means, the phase commutation is coordinated to a certain extent by basically following the exponential function, and the force ripple minimization is ensured in a wider range of switching position. This adaptive process can further extend to the single-phase excitation region in case that the current in the outgoing phase has not fallen to zero when it is turned OFF. The proposed adaptive FDF can be expressed as

$$\mathrm{FDF}_j(x) = \begin{cases} 0, & 0 \le x \le x_{\mathrm{on}} \\ F_{\mathrm{up\_}j}(x), & x_{\mathrm{on}} \le x \le x_{\mathrm{on}} + x_q \\ F_{\mathrm{dn\_}j}(x), & x_{\mathrm{on}} + x_q \le x \le x_{\mathrm{on}} + x_q + x_{\mathrm{ov}} \\ 0, & x_{\mathrm{on}} + x_q + x_{\mathrm{ov}} \le x \le x_p \end{cases} \tag{10}$$

$$F_{\mathrm{up\_}j}(x) = F_r - F_{\mathrm{est\_}j-1} \tag{11}$$

$$F_{\mathrm{dn\_}j}(x) = F_r \left[\exp\left(\frac{-(x - x_{\mathrm{on}} - x_q)^2}{x_{\mathrm{ov}}} \right) \right] \tag{12}$$

where F_r is the total force demand, $F_{\mathrm{est\_}j-1}$ is the estimated force of the outgoing phase, and $F_{\mathrm{up\_}j(x)}$ and $F_{\mathrm{dn\_}j(x)}$ denote the rising and declining distribution functions of the incoming phase, respectively. To verify the effectiveness of the proposed FDF, many simulations are carried out under the same force demand and switching positions with the exponential FDF. It can be observed from Fig. 10 that the force ripple is significantly reduced, compared with that of the conventional exponential FDF.

Although the force ripple is the dominant criterion of LSRA control for suspension application, other operation criteria, for example, the efficiency, are also critical for the system performance. The efficiency has a direct impact on the energy consumption of vehicles, particularly for the electric vehicles. Therefore, to obtain a high-performance active suspension system, the force ripple and operation efficiency are selected as the optimization criteria in this paper.

C. Hysteresis Force Control

The total force demand is distributed to four individual force references for each phase and compared with the estimated phase force, respectively. Thereby, the individual force of each phase is regarded as a control variable instead of the total force. The control signals were generated by a hysteresis force controller in response to the errors between the force reference and the estimated value of the corresponding phase. The phase commutation is considerably simplified by the separated force control algorithm. Because of the presence of mutual coupling when two adjacent phases are excited, the flux distribution and magnetic saturation are different from that of single-phase excitation mode as well as the ability of force output. Certain discrepancy between the estimated force and the actual force is introduced by ignoring the effect of mutual coupling. Since the force of each phase is estimated and controlled separately in this control method, the error could be increased during commutation, where two phases are excited simultaneously. However, this minor discrepancy is ignored for most practical purposes.

To improve the tracking accuracy and minimize the force ripple, a relative high-bandwidth hysteresis controller is needed in DIFC. However, it will increase the switching losses and sensitivity to signal noise. There is a tradeoff to determine the hysteresis band. The force dynamics for the magnetizing, freewheeling, and demagnetizing states and noise immunity margin should be carefully examined. It is practical to alter and optimize the hysteresis band by comparing the experimental results.

D. Switching Parameter Optimization

Although force ripple minimization is achieved over a wider range of switching parameters, the efficiency can be considerably different for the various selections of switching positions. Therefore, the turn-ON and turn-OFF positions can be optimized to improve the operation efficiency based on the force demand and motion speed. Because LSRA is basically operated below the base speed in the active suspension system, the impact of speed is not considered in this paper.

For motoring operation, it can be observed from Fig. 11 that the RMS phase current is insensitive to the change of turn-OFF position. Thus, the efficiency is decided by the selection of turn-ON position. The optimal value is determined as the excitation

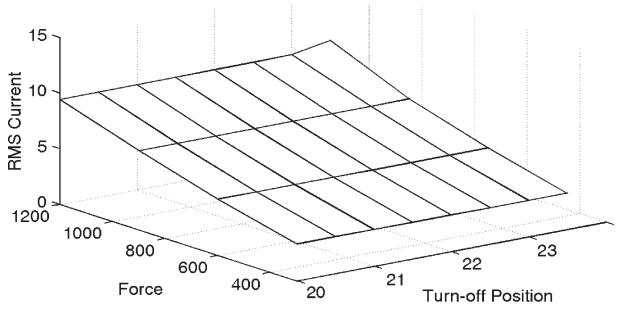

Fig. 11. Effects of turn-OFF position

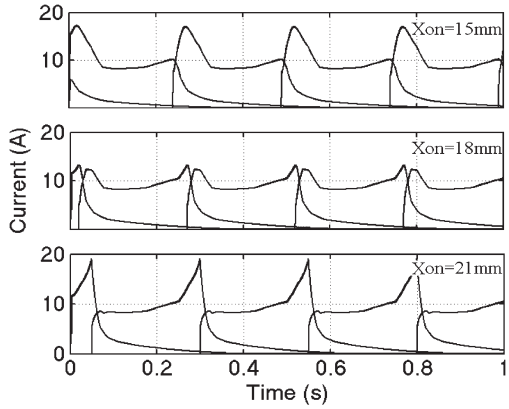

Fig. 12. Current profile at different turn-ON positions.

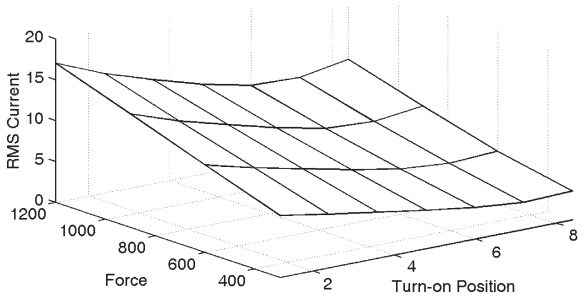

Fig. 13. Effects of turn-ON position.

current is built up when entering the effective force region. Certain advance or delay will result in increased peak and RMS current, as shown in Fig. 12. Moreover, the advance turn-ON position will extend the conductive region, thus increasing the RMS current. The optimal turn-ON position can be obtained from Fig. 13. It can be observed that the turn-ON position with the lowest RMS current is advanced gradually with the increase of force demand. It is because that more time is required to build up the higher phase current.

For the regenerating operation, the aim is to keep the force profile smooth during commutation and reduce the force ripple; hence, the improvement of efficiency is subject to the primary objective, which is different from the control strategy of the other switched reluctance generator. It can be observed from Fig. 14 that both switching positions contribute to the RMS phase current. The efficiency is basically increased with the decrease of turn-ON and turn-OFF positions. Although the lowest RMS current is obtained when the phase is turned-OFF at 36 mm, the force ripple deteriorates because of the lack of an overlap region of neighboring phases.

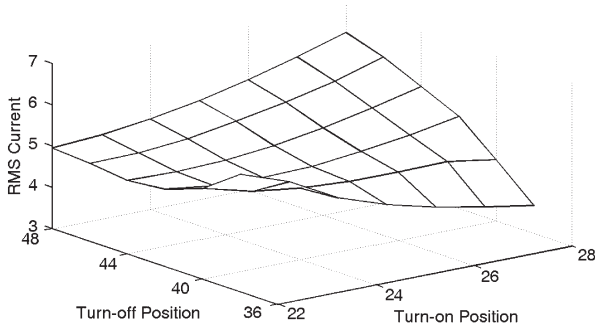

Fig. 14. Effects of switching positions.

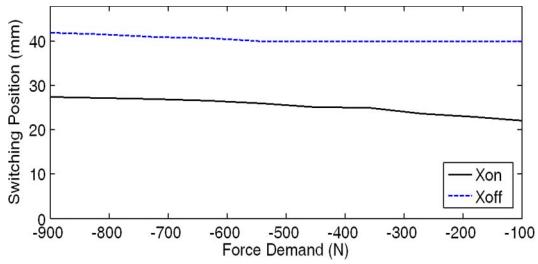

Fig. 15. Optimal switching positions in regenerative operation.

As demonstrated in Fig. 15, the optimal turn-ON position in regenerative operation is increased as the growth of force demand. The turn-OFF position remains constant at low force demand and then increases to ensure an adequate overlap region as the force demand gets larger.

The effective force regions of neighboring phases are overlapped to ensure the two-phase excitation simultaneously during the phase commutation. It makes the FDF an effective way to reduce the force ripple. By distributing the force demand between two neighboring phases, the phase force is individually regulated and varied smoothly with the translator position.

IV. Experimental Results

The performance of the DIFC strategy has been experimentally verified based on the dSPACE DS1104 controller board. A linear variable differential transformer (LVDT) position sensor was installed inside the LSRA to measure the translator position. To obtain the static force profile and construct the force estimator, a load cell was implemented to measure the force in a step of 2 mm under the excitation current from 2 to 20 A. The LSRA is placed vertically when testing with load and the regenerative operation mode. The external force can be varied with the different weights attached to the translator.

First, to compare the performance of proposed adaptive FDF, the experimental results with exponential FDF and without FDF are illustrated in Figs. 16 and 17, respectively. The control method without FDF means that the force of two neighboring phases is regulated indirectly by comparing the total force during commutation. The experimental force and current profile

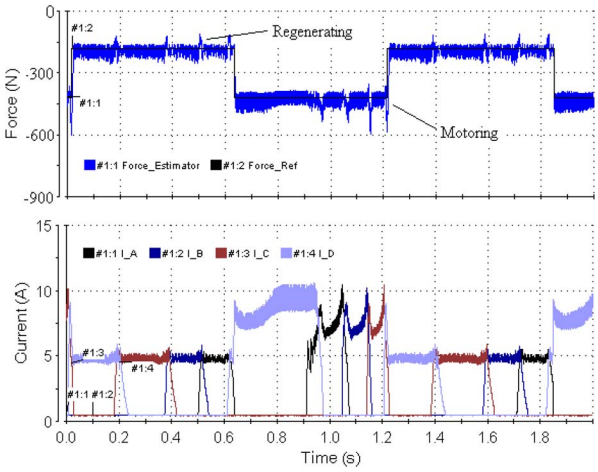

Fig. 16. Estimated force and measured current profiles with exponential FDF.

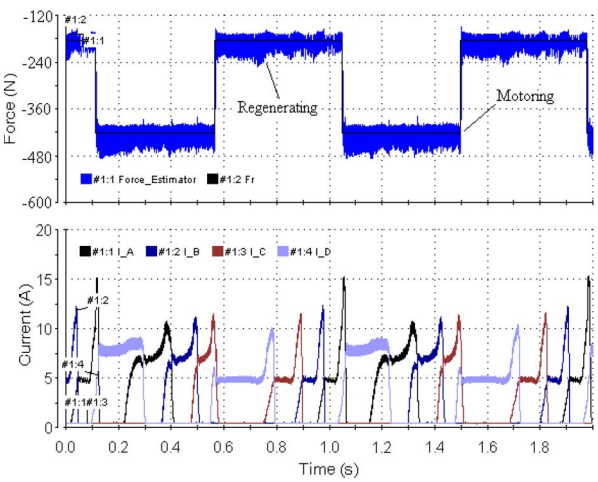

Fig. 17. Estimated force and measured current profiles without FDF.

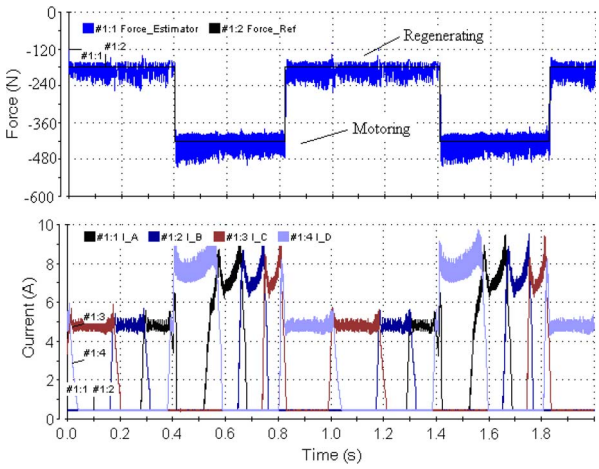

Fig. 18. Estimated force and measured current profiles with adaptive FDF.

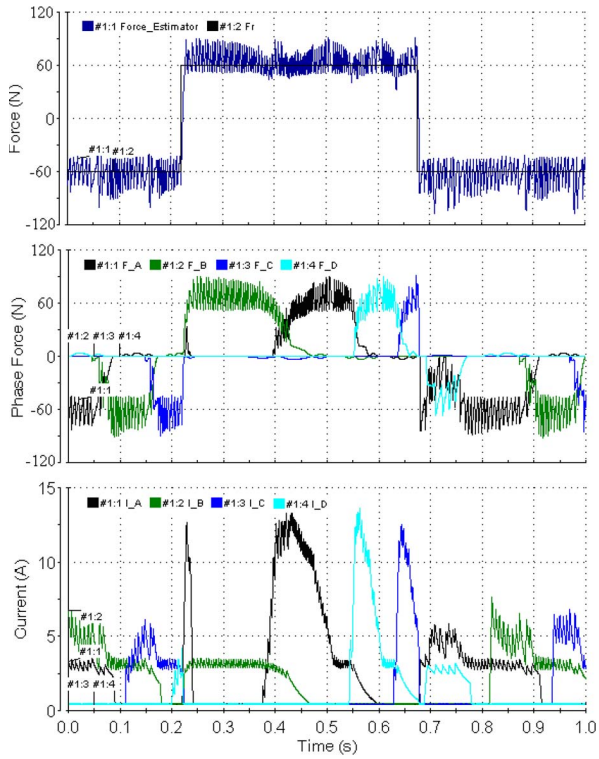

Fig. 19. Experimental results with advance turn-ON position.

with adaptive FDF are shown in Fig. 18. Three experiments were carried out in both the motoring and regenerating modes under the same external force and switching positions. The external force for regeneration is exerted by the gravity of the translator itself and the load attached to it. The translator is first controlled in motoring operation to move upward, and then move downward by the effect of gravity. Meanwhile, the LSRA is operated in regenerative mode and produces an upward force. The operation mode changes between modes I and IV. Hence, the sign of force in both motoring and regenerating is negative. It can be observed that the force profile of the exponential FDF is significantly deteriorated during phase commutation at both operation modes, although the RMS current is relative low. The force ripple without FDF is reduced, but at the cost of high peak and RMS phase current. In contrast, the force ripple minimization is achieved with higher efficiency by the application of an adaptive FDF. Because the force characteristics under low excitation current are relatively flat between 8 and 22 mm, which is the operating region of generating mode, there is no need for a much higher phase current at both turn-ON and turn-OFF positions for a low force demand. Hence, the phase current seems flat top in generating mode.

Further experimental tests are conducted to verify the commutation optimization process. The LSRA is placed horizontally and controlled to move back and forth continuously. The operation mode is changed between modes I and III. Therefore, the force profile oscillated between positive and negative. Several combinations of switching parameters were implemented under a variation of force demand. The experimental results of total force, phase force, and excitation current with different switching positions are demonstrated in Figs. 19 and 20. It can be observed that the force profiles of two switching conditions have similar shapes with reduced force ripple, whereas the RMS force current with advance turn-ON position is much greater than that with optimal turn-ON position. Figs. 18 and 21 illustrate the optimal response at a different force demand. The

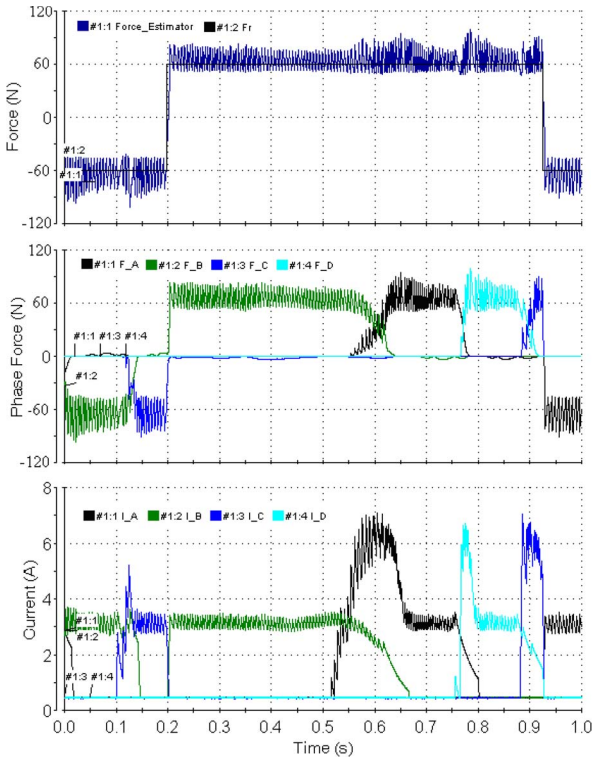

Fig. 20. Experimental results with optimal turn-ON position.

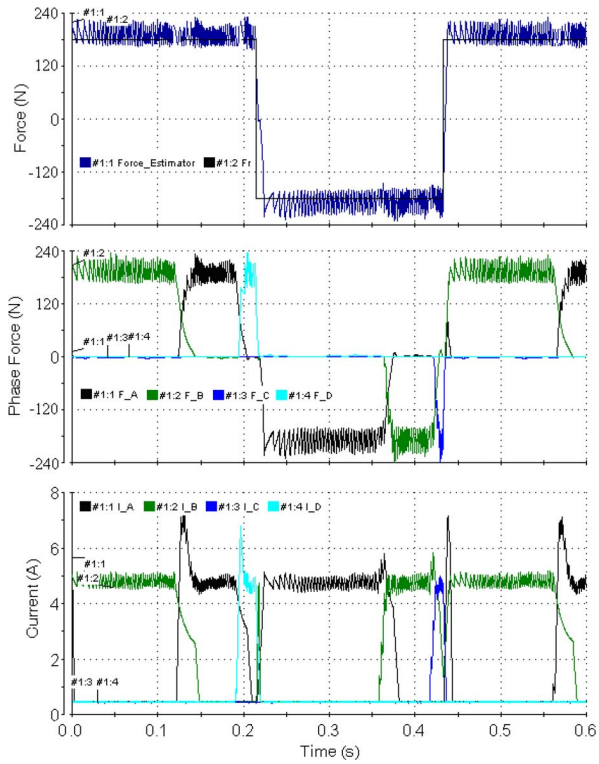

Fig. 21. Experimental results with higher force demand.

experimental results are consistent with the theoretical analysis and simulation results. Therefore, it is very practical to change the switching parameters under different operation conditions.

Fig. 22 compares the operation efficiencies under optimal and normal switching positions over a wide range of force

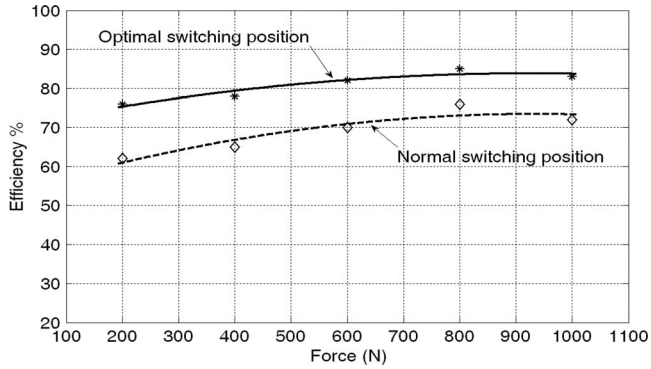

Fig. 22. Efficiency improvement with switching position optimization.

demand. Since the force ripple minimization is the primary objective, the comparison of efficiency is conducted among situations with acceptable force ripple. It can be observed that the operation efficiency is improved considerably by optimizing the switching parameters, and the efficiencies under both modes are enhanced as the force demand increased.

V. Conclusion

For application in the active suspension system, an improved DIFC has been investigated in this paper for four-quadrant operation of LSRA. This control strategy is composed of instantaneous force estimation, force demand distribution, hysteresis force control, and commutation optimization. An adaptive FDF is proposed to minimize the force ripple during phase commutation. Efficiency is then improved by online optimization of the switching parameters in the premise of ensuring minimum force ripple. The effectiveness of the proposed strategy is verified by both simulation and experimental results.

Appendix

Parameters of the LSRA used in the experimentation:

Number of module:	4
Number of phase:	4
Number of stator pole per module:	16
Number of translator pole:	8
Stator pole pitch:	36 mm
Translator pole pitch:	48 mm
Stator pole width:	13 mm
Translator pole width:	17 mm
Stator pole height:	49 mm
Stator yoke thickness:	13 mm
Stack length:	43 mm

References

[1] I. Martins, J. Esteves, G. D. Marques, and F. Pina da Silva, "Permanent-magnets linear actuators applicability in automobile active suspensions," *IEEE Trans. Veh. Technol.*, vol. 55, no. 1, pp. 86–94, Jan. 2006.

[2] B. L. J. Gysen, J. J. H. Paulides, J. L. G. Janssen, and E. A. Lomonova, "Active electromagnetic suspension system for improved vehicle dynamics," *IEEE Trans. Veh. Technol.*, vol. 59, no. 3, pp. 1156–1163, Mar. 2010.

[3] J. Wang, W. Wang, and K. Atallah, "A linear permanent-magnet motor for active vehicle suspension," *IEEE Trans. Veh. Technol.*, vol. 60, no. 1, pp. 55–63, Jan. 2011.
[4] W. D. Jones, "Easy ride: Bose Corp. uses speaker technology to give cars adaptive suspension," *IEEE Spectr.*, vol. 42, no. 5, pp. 12–14, May 2005.
[5] R. Krishnan, *Switched Reluctance Motor Drives: Modeling, Simulation, Analysis, Design, and Application*. Boca Raton, FL: CRC, 2001.
[6] B. L. J. Gysen, T. P. J. van der Sande, J. J. H. Paulides, and E. A. Lomonova, "Efficiency of a regenerative direct-drive electromagnetic active suspension," *IEEE Trans. Veh. Technol.*, vol. 60, no. 4, pp. 1384–1393, May 2011.
[7] M. Montazeri-Gh and M. Soleymani, "Investigation of the energy regeneration of active suspension system in hybrid electric vehicles," *IEEE Trans. Ind. Electron.*, vol. 57, no. 3, pp. 918–925, Mar. 2010.
[8] Z. Gang Sun, N. C. Cheung, S. W. Zhao, and W.-C. Gan, "Magnetic analysis of switched reluctance actuators in levitated linear transporters," *IEEE Trans. Veh. Technol.*, vol. 59, no. 9, pp. 4280–4288, Nov. 2010.
[9] H. S. Lim, R. Krishnan, and N. S. Lobo, "Design and control of a linear propulsion system for an elevator using linear switched reluctance motor drives," *IEEE Trans. Ind. Electron.*, vol. 55, no. 2, pp. 534–542, Feb. 2008.
[10] W.-C. Gan, N. C. Cheung, and L. Qiu, "Position control of linear switched reluctance motors for high-precision applications," *IEEE Trans. Ind. Appl.*, vol. 39, no. 5, pp. 1350–1362, Sep./Oct. 2003.
[11] S. W. Zhao, N. C. Cheung, W.-C. Gan, J. M. Yang, and J. F. Pan, "A self-tuning regulator for the high-precision position control of a linear switched reluctance motor," *IEEE Trans. Ind. Electron.*, vol. 54, no. 5, pp. 2425–2434, Oct. 2007.
[12] A. A. Goldenberg, I. Laniado, P. Kuzan, and C. Zhou, "Control of switched reluctance motor torque for force control applications," *IEEE Trans. Ind. Electron.*, vol. 41, no. 4, pp. 461–466, Aug. 1994.
[13] I. Husain, "Minimization of torque ripple in SRM drives," *IEEE Trans. Ind. Electron.*, vol. 49, no. 1, pp. 28–39, Feb. 2002.
[14] R. B. Inderka and R. W. A. A. De Doncker, "DITC-direct instantaneous torque control of switched reluctance drives," *IEEE Trans. Ind. Appl.*, vol. 39, no. 4, pp. 1046–1051, Jul./Aug. 2003.
[15] F. Daldaban and N. Ustkoyuncu, "A new double sided linear switched reluctance motor with low cost," *Energy Convers. Manage.*, vol. 47, no. 18/19, pp. 2983–2990, Nov. 2006.
[16] S. K. Sahoo, S. K. Panda, and J. X. Xu, "Direct torque controller for switched reluctance motor drive using sliding mode control," in *Proc. PEDS*, 2005, pp. 1129–1134.
[17] R. B. Inderka, R. W. De Doncker, and M. Krehenbrink, "On-line estimation of instantaneous torque in switched reluctance machine control," in *Proc. IEEE ISIE*, 2000, pp. 385–389.
[18] Z. Lin, D. S. Reay, B. W. Williams, and X. He, "On-line torque estimation in a switched reluctance motor for torque ripple minimisation," in *Proc. IEEE Int. Symp. Ind. Electron.*, 2004, pp. 981–985.
[19] T. J. E. Miller, *Electronic Control of Switched Reluctance Machines*. Boston, MA: Newnes, 2001.
[20] Z. Lin, D. S. Reay, B. W. Williams, and X. He, "Online modeling for switched reluctance motors using B-spline neural networks," *IEEE Trans. Ind. Electron.*, vol. 54, no. 6, pp. 3317–3322, Dec. 2007.
[21] S. Paramasivam and R. Arumugam, "Hybrid fuzzy controller for speed control of switched reluctance motor drives," *Energy Convers. Manage.*, vol. 46, no. 9/10, pp. 1365–1378, 2005.
[22] D. S. Schramm, B. W. Williams, and T. C. Green, "Torque ripple reduction of switched reluctance motors by phase current optimal profiling," in *Proc. 23rd Annu. IEEE PESC*, 1992, pp. 857–860.
[23] I. Husain and M. Ehsani, "Torque ripple minimization in switched reluctance motor drives by PWM current control," *IEEE Trans. Power Electron.*, vol. 11, no. 1, pp. 83–88, Jan. 1996.
[24] S. K. Sahoo, S. K. Panda, and J.-X. Xu, "Indirect torque control of switched reluctance motors using iterative learning control," *IEEE Trans. Power Electron.*, vol. 20, no. 1, pp. 200–208, Jan. 2005.
[25] M. Ilic-Spong, T. J. E. Miller, S. R. Macminn, and J. S. Thorp, "Instantaneous torque control of electric motor drives," *IEEE Trans. Power Electron.*, vol. PEL-2, no. 1, pp. 55–61, Jan. 1987.
[26] X. D. Xue, K. W. E. Cheng, and S. L. Ho, "Optimization and evaluation of torque-sharing functions for torque ripple minimization in switched reluctance motor drives," *IEEE Trans. Power Electron.*, vol. 24, no. 9, pp. 2076–2090, Sep. 2009.

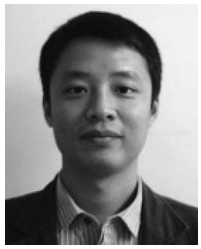

Zhu Zhang (S'11) received the M.Eng. degree from the South China University of Technology, Guangzhou, China, in 2004. He is currently working toward the Ph.D. degree with the Department of Electric Engineering, The Hong Kong Polytechnic University, Kowloon, Hong Kong.

He had been a Research Assistant with the Department of Electric Engineering, The Hong Kong Polytechnic University. His research interests include motor design and power electronics.

N. C. Cheung (S'85–M'91–SM'05) received the B.Sc. degree from the University of London, London, U.K., in 1981, the M.Sc. degree from the University of Hong Kong, Kowloon, Hong Kong, in 1987, and the Ph.D. degree from the University of New South Wales, Kensington, Australia, in 1996.

He was a Technical Manager with ASM Assembly Automation Ltd., Hong Kong, for two years, where he worked in the areas of intelligent motion control and robotics systems. He has been with the Hong Kong Polytechnic University, Kowloon, Hong Kong, since 1997, where he is currently with the Department of Electrical Engineering.

Dr. Cheung is a Chartered Engineer in the U.K. and a member of the Institution of Engineering and Technology, U.K.

K. W. E. Cheng (M'90–SM'06) received the B.Sc. and Ph.D. degrees from the University of Bath, Bath, U.K., in 1987 and 1990, respectively.

He was a Principal Engineer with Lucas Aerospace, U.K., where he led a number of power electronics projects before he joined the Hong Kong Polytechnic University, Kowloon, Hong Kong, in 1997, where he is currently a Professor and the Director of the Power Electronics Research Centre. He is the author of over 250 published papers and seven books. His research interests include power electronics, motor drives, electromagnetic interference, electric vehicles, and energy saving.

Dr. Cheng received the Institution of Electrical Engineers Sebastian Z. De Ferranti Premium Award in 1995, the Outstanding Consultancy Award in 2000, the Faculty Merit Award for Best Teaching in 2003 from the Hong Kong Polytechnic University, the Faculty Engineering Industrial and Engineering Services Grant Achievement Award in 2006, the Brussels Innova Energy Gold Medal With Mention in 2007, the Consumer Product Design Award in 2008, and the Electric Vehicle Team Faculty Merit Award in 2009.

Xiangdang Xue (M'10) received the B.Eng. degree in electrical engineering from Hefei University of Technology, Hefei, China, in 1984, the M.Eng. degree in electrical engineering from Tianjin University, Tianjin, China, in 1987, and the Ph.D. degree in electrical engineering from the Hong Kong Polytechnic University, Kowloon, Hong Kong, in 2004.

He was a Lecturer and an Associate Professor with the Department of Electrical Engineering, Tianjin University, from 1987 to 2001, where he was engaged in teaching and research. He is currently a Research Fellow with the Department of Electrical Engineering, Hong Kong Polytechnic University. He is the author of over 70 published papers. His research interests include electrical machines, electrical drives, and power electronics. His current research is focused on electric machines and drives applied to electric vehicles and wind-power generations.

Jiongkang Lin is currently working toward the Ph.D. degree.

He had been a Research Assistant with the Department of Electrical Engineering, The Hong Kong Polytechnic University, Kowloon, Hong Kong. His research interests include power electronics.